BIOCHEMISTRY

SMARCAD1 is an ATP-dependent histone octamer exchange factor with de novo nucleosome assembly activity

Jonathan Markert[1], Keda Zhou[1], Karolin Luger[1,2]*

Copyright © 2021 The Authors, some rights reserved; exclusive licensee American Association for the Advancement of Science. No claim to original U.S. Government Works. Distributed under a Creative Commons Attribution NonCommercial License 4.0 (CC BY-NC).

The adenosine 5′-triphosphate (ATP)–dependent chromatin remodeler SMARCAD1 acts on nucleosomes during DNA replication, repair, and transcription, but despite its implication in disease, information on its function and biochemical activities is scarce. Chromatin remodelers use the energy of ATP hydrolysis to slide nucleosomes, evict histones, or exchange histone variants. Here, we show that SMARCAD1 transfers the entire histone octamer from one DNA segment to another in an ATP-dependent manner but is also capable of de novo nucleosome assembly from histone octamer because of its ability to simultaneously bind all histones. We present a low-resolution cryo–electron microscopy structure of SMARCAD1 in complex with a nucleosome and show that the adenosine triphosphatase domains engage their substrate unlike any other chromatin remodeler. Our biochemical and structural data provide mechanistic insights into SMARCAD1-induced nucleosome disassembly and reassembly.

INTRODUCTION

DNA in eukaryotic cells is packaged by wrapping around octamers of the four core histones (H2A-H2B and H3-H4) to form nucleosomes (*1*). These present a major barrier to DNA-dependent polymerases during transcription, replication, and repair. Adenosine 5′-triphosphate (ATP)–dependent chromatin remodelers slide, evict, or transfer ("exchange") histones to either space nucleosomes to locally increase DNA accessibility or to incorporate histone variants in place of major-type histones (*2*). The reactions catalyzed by the various remodelers, and their outcomes, depend on the type of remodeler and on the assays and substrates used. For example, SWI2/SNF2-Related 1 Chromatin Remodeling Complex (SWR1) recognizes H2A containing nucleosomes and, in the presence of H2A.Z and ATP, removes H2A-H2B and replaces it with a histone variant dimer H2A.Z-H2B (histone exchange) (*3*). Inositol auxotrophy 80 complex (INO80), which is closely related to SWR1, slides nucleosomes along the DNA (*4*), while Remodeling the Structure of Chromatin complex slides nucleosomes but can also evict the histone octamer from DNA under certain conditions (*5*).

SMARCAD1 is a member of the INO80 family that is found throughout the genome and is implicated in DNA replication, transcription, and DNA damage repair (*6*–*14*). SMARCAD1 is of therapeutic interest because of its up-regulation and/or mutation in pancreatic and breast cancer (*15*, *16*). Human SMARCAD1 consists of two N-terminal Coupling of Ubiquitin to ER degradation (CUE) domains and a split catalytic domain [consisting of adenosine triphosphatase 1 (ATPase 1) and ATPase 2] that are connected by an extended loop that led to its classification into the INO80 family (*17*, *18*). The N-terminal CUE domains (specifically CUE 1) interact with binding partners to help recruit SMARCAD1 throughout the genome (*19*, *20*), while the C-terminal catalytic domain is required for maintaining genome integrity (*21*, *22*). While progress has been made regarding biological function, little is known about overall structure and interactions of human SMARCAD1, and only a few functional studies have been published with the *Saccharomyces cerevisiae* and *Schizosaccharomyces pombe* homologs Fun30 and Fft3. Fft3 is found at open reading frames of *S. pombe* genes and contributes to the eviction of histones from actively transcribed genes (*23*), while Fun30 and human SMARCAD1 appear to be primarily involved in histone eviction near sites of DNA damage to allow resection (*14*, *24*). Fun30 has also been implicated in telomeric silencing in yeast (*6*, *25*, *26*) and in the maintenance of heterochromatin (*27*). A recent role in maintaining replication fork stability has also been suggested (*28*). Fun30 has low nucleosome sliding activity but evicts and exchanges histone H2A-H2B dimers (and, to a lesser extent, entire histone octamer) between different DNA segments (*29*).

RESULTS

Recombinant SMARCAD1 requires dephosphorylation to bind nucleosomes

We purified SMARCAD1 (Fig. 1A) from Sf9 insect cells using the Bac-to-Bac baculovirus expression system (Fig. 1B). Using size exclusion chromatography coupled to multiangle light scattering (SEC-MALS), we determined that SMARCAD1 is a monomer with an apparent molecular weight of 129.5 kDa (fig. S1). Initial attempts to demonstrate interactions between SMARCAD1 and various nucleosome substrates were not successful. Because other remodelers are known to be regulated by Post-Translational Modifications (PTMs) (*30*, *31*), we analyzed SMARCAD1 for modifications that might have been added during expression in insect cells. Trypsin-digested SMARCAD1 was analyzed for phosphorylation sites (STY), and 23 sites were identified in the N terminus of SMARCAD1 (Fig. 1B). No sites were identified in the predicted ATPase domains.

Because phosphorylation of the Brahma-Associated Factor complex (BAF) complex is known to regulate its activity (*30*), we tested whether this was also the case for SMARCAD1. Phosphates were removed with calf intestinal alkaline phosphatase (CIP) followed by further purification. Dephosphorylated SMARCAD1 (from here on termed SMARCAD1) migrates with phosphorylated SMARCAD1 (pSMARCAD1) on SDS–polyacrylamide gel electrophoresis (SDS-PAGE) (Fig. 1B). Gel shift assays revealed a profound difference in

[1]Department of Biochemistry, University of Colorado Boulder, Boulder, CO 80303, USA. [2]Howard Hughes Medical Institute, Chevy Chase, MD 20815, USA.
*Corresponding author. Email: karolin.luger@colorado.edu

Downloaded from https://www.science.org on June 12, 2022

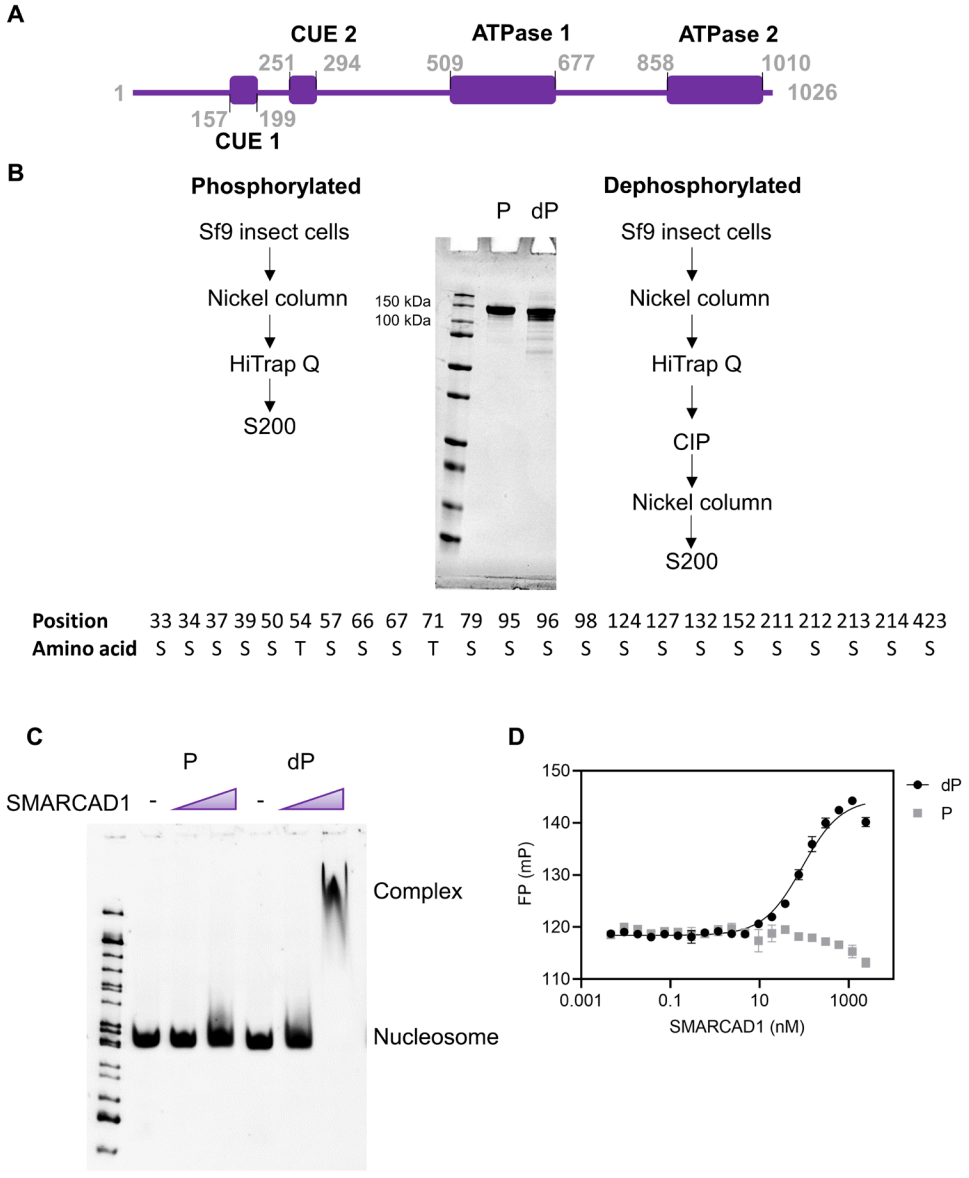

Fig. 1. SMARCAD1 purified from Sf9 cells is phosphorylated and requires dephosphorylation to bind nucleosomes. (**A**) Four known domains of SMARCAD1. (**B**) Purification scheme for phosphorylated and dephosphorylated SMARCAD1 (P and dP), and SDS-PAGE of purified proteins. Twenty-three phosphorylation sites were identified using MaxQuant. CIP, calf intestinal alkaline phosphatase. (**C**) Five percent native tris-borate EDTA (TBE) gel of 165-bp nucleosome (7 N11; 100 nM) mixed with 0, 100, or 1800 nM P SMARCAD1 or dP SMARCAD1. dP SMARCAD1 (1800 nM) binds the nucleosome as indicated by the upshift of the nucleosome band. (**D**) FP assay of P SMARCAD1 or dP SMARCAD1 (0 to 2500 nM) with 20 nM Alexa Fluor 488–labeled 7 N11 nucleosome. Dissociation constant (K_D) of P SMARCAD1 could not be determined; dP SMARCAD1 $K_{D,nuc} = 90 \pm 9$ nM. K_D and SE were determined from three replicates.

nucleosome binding activity between SMARCAD1 and pSMARCAD1. While pSMARCAD1 was unable to bind to DNA, or to a nucleosome reconstituted onto a 165–base pair (bp) DNA fragment (consisting of the 601 positioning sequence with 7 and 11 bp of DNA extending on either side; "7 N11"), SMARCAD1 caused a nucleosome shift in native PAGE (Fig. 1C). We quantified the interaction using a fluorescence polarization (FP) assay. A 7 N11 nucleosome was fluorescently labeled at H4 E63C with an Alexa Fluor 488 maleimide fluorophore. SMARCAD1 or pSMARCAD1 were then titrated, and the increase in FP signal was plotted (Fig. 1D). SMARCAD1 bound with an affinity of $K_{D,nuc} = 90 \pm 9$ nM, while pSMARCAD1 exhibited no binding. Because the ability of a remodeler to bind nucleosome is essential for its functions, all subsequent experiments were performed with dephosphorylated SMARCAD1.

SMARCAD1 prefers nucleosomes over free DNA for ATPase activation and exchanges histone octamers in an ATP-dependent manner

To test whether SMARCAD1 prefers nucleosomes over free DNA, we used the same FP assay as described in Fig. 1D, except that the nucleosome was labeled at H2B T115C with Alexa Fluor 488, and a 147-bp DNA fragment was labeled with Alexa Fluor 488. SMARCAD1

Downloaded from https://www.science.org on June 12, 2022

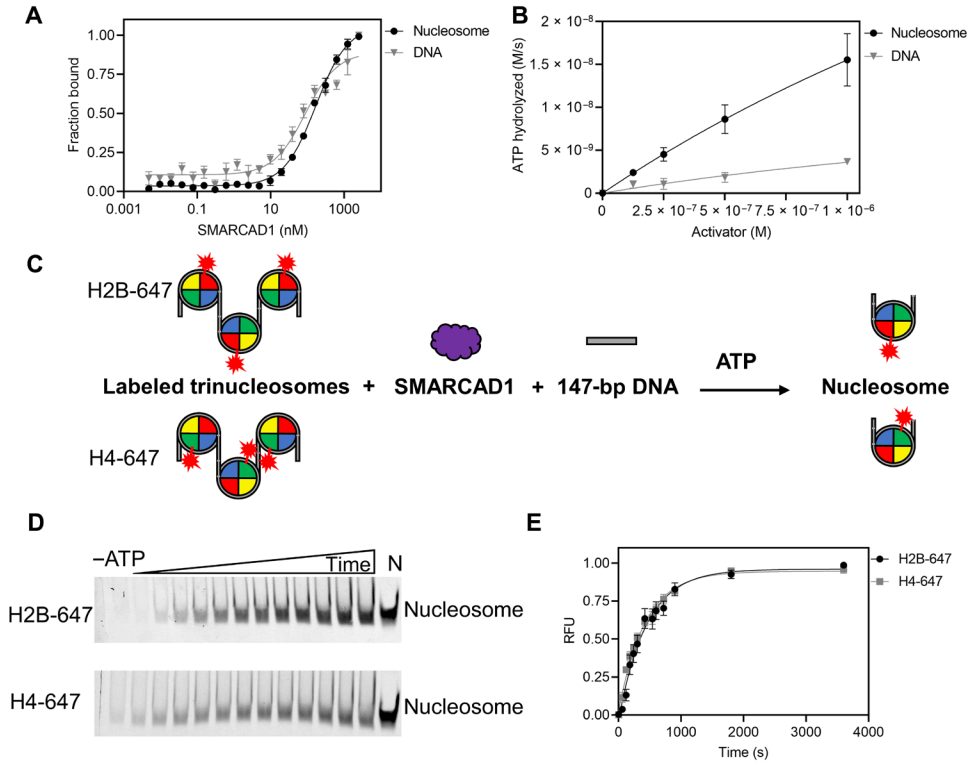

Fig. 2. SMARCAD1 is an ATP-dependent chromatin remodeler with histone exchange activity. (**A**) FP assay of SMARCAD1 (0 to 2500 nM) with 10 nM Alexa Fluor 488–labeled 7 N11 nucleosome or 10 nM Alexa Fluor 488–labeled 147-bp DNA. $K_{D,nuc} = 160 \pm 10$ nM; $K_{D,DNA} = 80 \pm 10$ nM. K_D and SE were determined from three replicates. (**B**) ATP hydrolysis assay of SMARCAD1 (100 nM) with 7 N11 nucleosome (0 to 1000 nM) or 165-bp DNA (0 to 1000 nM). SE bars on graph were determined from three replicates. (**C**) Schematic of histone exchange assay. SMARCAD1 (3 μM) was mixed with Atto647–labeled trinucleosomes [(30N60N60N30] (75 nM trinucleosome/225 nM mononucleosome) and 147-bp acceptor DNA (1.5 μM). Reactions were initiated with the addition of 1 mM ATP and quenched at indicated time points (fig. S3) with EDTA followed by visualization on a 5% native TBE gel. (**D**) Five percent native TBE gel of histone exchange assay [described in (C)] shows that in the absence of ATP (for 60-min time point), little H2B-647 or H4-647 is exchanged. When ATP is added and reaction is allowed to proceed 0 to 60 min, there is an increase in exchange, and product corresponds to nucleosome control. (**E**) Quantification of (D). SMARCAD1 exchanges both Atto647 H4 ($k_{obs,H4} = 2.2 \pm 0.2 \times 10^{-3}$ s^{-1}) and Atto647 H2B ($k_{obs,H2B} = 2.3 \pm 0.1 \times 10^{-3}$ s^{-1}) at the same rate. k_{obs} and SE were obtained from five replicates.

binds nucleosomes and DNA with similar affinities (Fig. 2A and fig. S2) ($K_{D,Nuc}$ = 160 ± 10 nM; $K_{D,DNA}$ = 80 ± 10 nM; also compare with the value for a different SMARCAD1 prep of $K_{D,nuc}$ = 90 ± 9 nM stated above).

Because all remodelers make several contacts with DNA (*2*), the ability of SMARCAD1 to bind free DNA is expected. To compare the potency of nucleosomes and free DNA in activating SMARCAD1 catalytic activity, we used an assay that couples ATP hydrolysis to NADH (reduced form of nicotinamide adenine dinucleotide) oxidation (Fig. 2B) (*4*). Addition of increasing amounts of DNA results in only a subtle increase in ATP hydrolysis, whereas nucleosome addition greatly stimulates ATP hydrolysis. Thus, despite the similar affinity for DNA and nucleosomes, the nucleosomes are much more potent than DNA in activating SMARCAD1 catalytic activity.

In vitro, Fun30 promotes histone exchange rather than sliding (*29*), while Fft3 evicts histones in actively transcribed regions (*23*). To test whether SMARCAD1 exhibits histone exchange activity, we prepared trinucleosomes (Fig. 2C) with either H2B or H4 carrying a fluorescent label. SMARCAD1 and 147-bp acceptor DNA were added; reactions were initiated by the addition of ATP and quenched with EDTA after the indicated times. The rate of histone transfer from trinucleosomes onto 147-bp acceptor DNA was determined by quantifying the appearance of a fluorescently labeled mononucleosome (Fig. 2, D and E, and fig. S3). In the absence of ATP, no histones were transferred, while in the presence of ATP, both H2B and H4 were transferred onto acceptor DNA to form particles that migrate like the nucleosome control. Intriguingly, both H2B and H4 are transferred to form mononucleosomes at identical rates (Fig. 2E), suggesting that the two histones are transferred together.

SMARCAD1 binds histones in the absence of DNA and functions as a nucleosome assembly factor

Our data predict that SMARCAD1 should bind histones in the absence of DNA, and this was tested using FP. Refolded histones (H3-H4* and H2A-H2B*, labeled* with Alexa Fluor 488) were mixed separately and incubated with increasing amounts of SMARCAD1 (Fig. 3, A and B). The observed increase in FP for H3H4 (Fig. 3A; $K_{D,H3H4} = 4 \pm 1$ nM) and H2AH2B (Fig. 3B; $K_{D,H2AH2B} = 10 \pm 2$ nM) reveals that SMARCAD1 interacts with individual histones.

Because H3H4 and H2AH2B are exchanged at the same rate (Fig. 2E), our data also suggest that SMARCAD1 simultaneously binds all histones in the absence of DNA. This was tested using fluorescence resonance energy transfer (FRET). Histones H3-H4 and H2A-H2B do not interact under physiological conditions in the absence of DNA. Refolded histones (H3-H4* and H2A-H2B*,

Downloaded from https://www.science.org on June 12, 2022

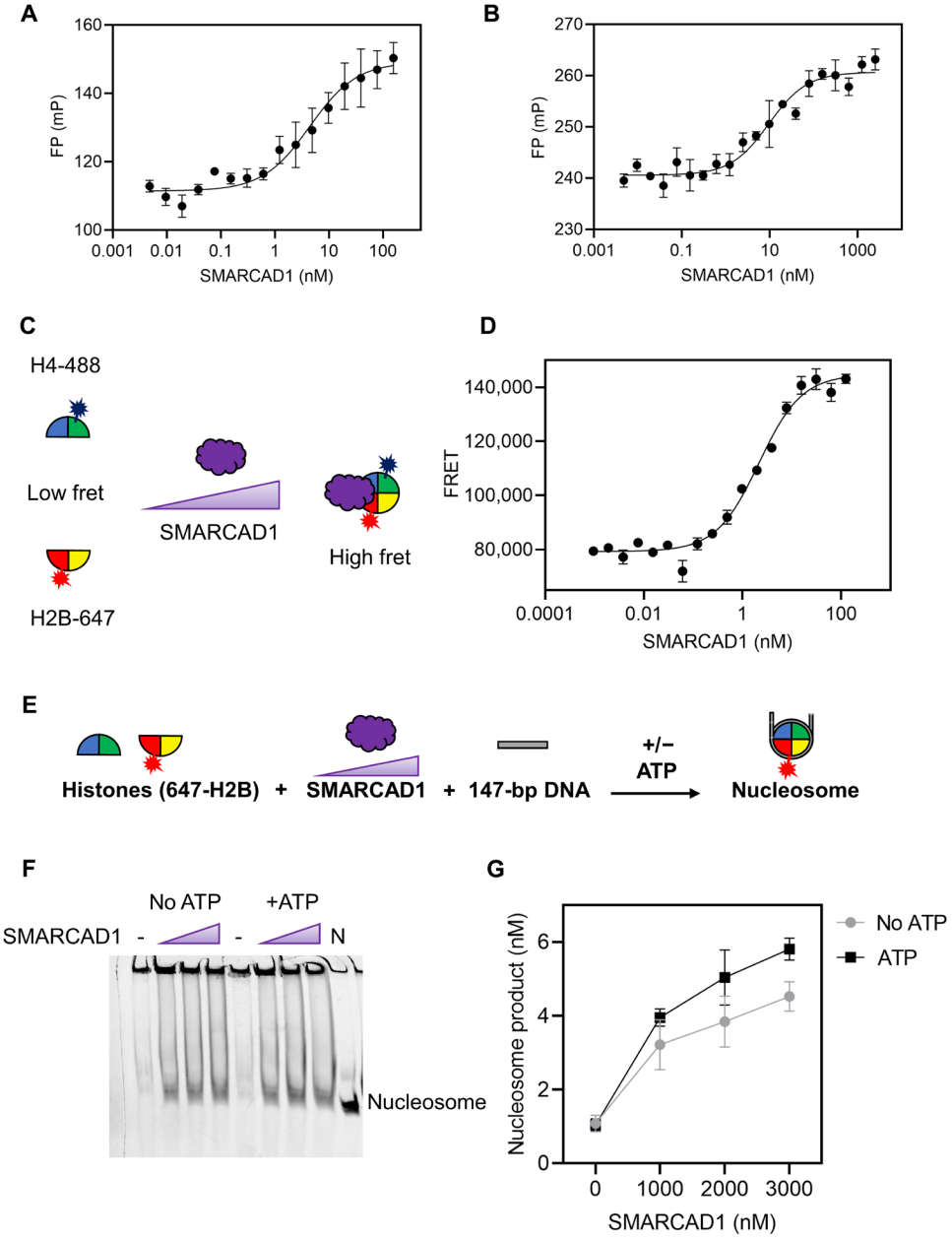

Fig. 3. SMARCAD1 binds histones and assembles nucleosomes independently of ATP. (**A**) FP assay reveals SMARCAD1 (0 to 156 nM) binds H3-H4 (Alexa Fluor 488–H4, 5 nM) in the absence of H2A-H2B or DNA with high affinity ($K_{D,H3H4} = 4 \pm 1$ nM). K_D and SE come from three replicates. (**B**) FP assay reveals that SMARCAD1 (0 to 2500 nM) binds H2A-H2B (Alexa Fluor 488–H2B, 5 nM) in the absence of H3-H4 or DNA with high affinity ($K_{D,H2AH2B} = 10 \pm 2$ nM). K_D and SE come from three replicates. (**C**) Schematic of FRET-based histone binding assay. To monitor histone binding, H3-H4 (Alexa Fluor 488–H4) and H2A-H2B (Atto647N H2B) were mixed at 10 nM. SMARCAD1 was titrated to histones (0 to 125 nM), and the increase in FRET signal is measured. (**D**) SMARCAD1 binds histones in the absence of DNA with high affinity ($K_{D,histones} = 1.3 \pm 0.4$ nM). K_D and SE were obtained from three replicates. (**E**) Schematic of nucleosome assembly reaction. H3-H4 and H2A-H2B (50 nM; 647-H2B) are mixed with SMARCAD1 (0 to 3 μM) for 15 min followed by addition of 147-bp DNA (50 nM) that was incubated for a further 15 min with and without 1 mM ATP. Reactions were quenched with pUC-19 plasmid DNA and then analyzed on a 5% native TBE gel. (**F**) In the absence of SMARCAD1, little histones are assembled onto DNA; however, after addition of SMARCAD1, there is an increase in nucleosome assembly. Nucleosome assembly happens both in the presence and absence of ATP. (**G**) Quantification of gel from (F) reveals that SMARCAD1 assembles nucleosomes equally well in the presence or absence of 1 mM ATP. SE bars in graph are from three replicates.

labeled* with Alexa Fluor 488 and Atto647N, respectively) were combined at low concentrations and incubated with increasing amounts of SMARCAD1 (Fig. 3C). The observed increase in FRET ($K_{D,histones}$ = 2.1 ± 0.1 nM) demonstrates that SMARCAD1 brings together histones H2B and H4 in the absence of DNA (Fig. 3D).

Results shown in Fig. 2 (D and E) indicate that SMARCAD1 transfers both H2A-H2B and H3-H4 from one DNA fragment to another. To test whether SMARCAD1 promotes de novo nucleosome assembly (without first taking them off another DNA fragment), we preincubated SMARCAD1 with a mixture of H2A-H2B (Atto647)

Downloaded from https://www.science.org on June 12, 2022

and H3-H4, and then added 147-bp DNA (Fig. 3E). The appearance of fluorescent nucleosomes on a native gel was then quantified. In the absence of SMARCAD1, only minor amounts of nucleosomes were formed. As SMARCAD1 is added, the nucleosome band intensifies (Fig. 3, F and G). Unlike for the reaction shown in Fig. 2, where histones must first be removed from DNA in an ATP-dependent manner, ATP is not required for the nucleosome assembly reaction that starts with free histone complexes.

SMARCAD1 interacts with nucleosomes in a unique manner

We determined the cryo–electron microscopy (cryo-EM) structure of SMARCAD1 bound to a nucleosome at an overall resolution of ~6.5 Å (fig. S4). Upon optimization, we ultimately used a nucleosome substrate with 70-bp extranucleosomal DNA extending from one side (0 N70). To further stabilize the complex, we used GraFix with glutaraldehyde (*32*). In addition, a nonhydrolyzable ATP analog [prepared by combining adenosine 5′-diphosphate (ADP) with $BeSO_4$ and NaF to form ADP-BeF_3] (*33*) was used to further stabilize the complex, as shown for other remodelers before (*34*).

The density for the nucleosome was well defined and could be visualized at ~5 Å, making placement of the human nucleosome [Protein Data Bank (PDB): 2CV5] straightforward (Fig. 4). We also observed density for ~20 of the 70-bp extranucleosomal DNA. The density for SMARCAD1 was at ~10 Å, and thus, we were unable to confidently build a high-resolution model of SMARCAD1, as no structure of SMARCAD1 in isolation is available. We used SWISS-MODEL to predict a structure of the SMARCAD1 ATPase domain using Imitation switch (Iswi) (PDB: 5JXR) as a template (*35*). This model was then fit into the EM map. Although we used full-length SMARCAD1 for grid preparation, we only see density corresponding to the C-terminal catalytic domain encompassing ATPase 1 and ATPase 2 (Fig. 4).

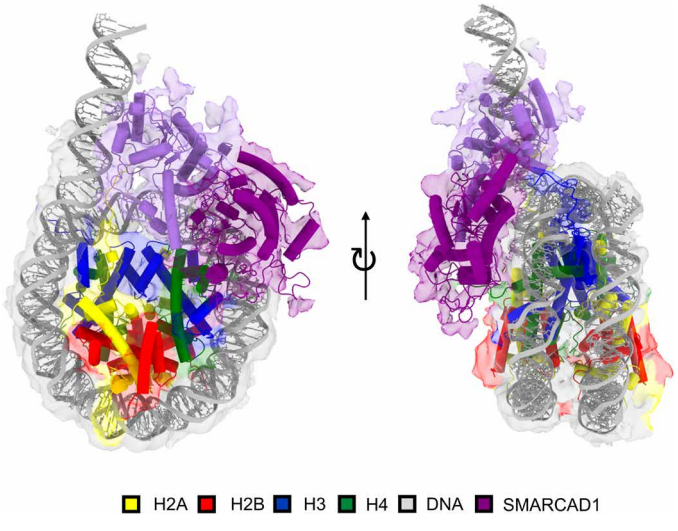

Fig. 4. Cryo-EM structure of the SMARCAD1-nucleosome complex, revealing a unique binding mode. SMARCAD1 makes interactions with extranucleosomal DNA, the nucleosomal dyad (SHL 0), and SHL −1, as well with the H4 N-terminal tail and the H3 N-terminal tail. Although full-length SMARCAD1 was used for cryo-EM sample preparation, only the C-terminal catalytic domain (amino acids 509 to 1026) was visible in the map. To improve clarity, the "surface dust" command was used in ChimeraX to remove noise from maps.

The low resolution of SMARCAD1 precludes interpretation of the molecular interactions, but we can draw conclusions from overall nucleosomal interactions. The C-terminal catalytic domain of SMARCAD1 interacts with the nucleosome at several distinct contact points [DNA locations on the nucleosome are defined by their superhelix location, or SHL, where SHL 0 denotes the nucleosomal dyad, cartoon in Fig. 4; (*1*)]. The SMARCAD1 motor sits on top of SHL 0 where it covers ~10 bp of nucleosomal DNA. It interacts with ~10 bp of the extranucleosomal DNA and reaches toward SHL 0. SMARCAD1 continues to interact with DNA at the dyad axis but also maintains contact with DNA near SHL −1 (movie S1). The remaining ~500 amino acids of SMARCAD1 for which no density is observed is predicted to be largely disordered. The overall architecture of the nucleosome is unchanged compared to unbound nucleosome in the main class (Fig. 4).

We identified a second class of particles at ~6.2 Å (map 2) (fig. S4). In this class, there is no discernable difference in how SMARCAD1 interacts with the nucleosome nor are there any structural rearrangements in the histones, but nucleosomal DNA on the distal side of SMARCAD1 is peeled away from the histone core starting near SHL +4 (fig. S5). This is probably due to spontaneous unwrapping of DNA ends previously observed on EM grids (*36*), although we cannot exclude that SMARCAD1 contributes to this destabilization.

SMARCAD1 requires both H3 and H4 N-terminal tails for catalytic activity

The catalytic domain of SMARCAD1 is placed to allow it to make direct contacts with the H4 and H3 N-terminal tails (Figs. 4 and 5, A and B, and movie S1), although the molecular details of the interaction remain to be determined. In light of this finding and given the established importance of histone tails in regulating the activity of other chromatin remodelers (*2*, *37*–*39*), we tested their contribution to SMARCAD1 catalytic activity. SMARCAD1 binds nucleosomes reconstituted with tailless (TL) histones H3 or H4 (TLH3 and TLH4) with the same affinity as it binds nucleosomes with full-length histones (Fig. 5C and fig. S2). However, ATP hydrolysis is significantly reduced when stimulated by TLH4 nucleosomes (Fig. 5D), and consequently, the histone exchange activity for TLH4 nucleosomes is abolished (Fig. 5, E and F, and fig. S6). In contrast, removal of the H3 tail does not affect ATP hydrolysis (Fig. 5D), yet the relative amount of histone exchange is significantly reduced in TLH3 compared to wild type (WT) (Fig. 5, E and F, and fig. S6). To ensure that the lack in exchange activity in TLH3 and TLH4 is not simply due to the inability of SMARCAD1 to interact with histones, we demonstrate that SMARCAD1 assembles TLH3 and TLH4 nucleosomes from histone complexes (de novo nucleosome assembly activity; fig. S7, A and B).

DISCUSSION

Different ATP-dependent chromatin remodelers engage their nucleosome substrate in a variety of ways, but, with the exception of INO80, the structurally conserved ATPase domains of all known remodelers contact nucleosomal DNA at SHL 2 (*2*). SMARCAD1, a single-subunit chromatin remodeler from the INO80 family, is unique in that its ATPase motor sits astride SHL 0 and binds DNA at SHL −1 while, at the same time, engaging extranucleosomal linker DNA (Fig. 4). The ATPase domains of Iswi, which served

Downloaded from https://www.science.org on June 12, 2022

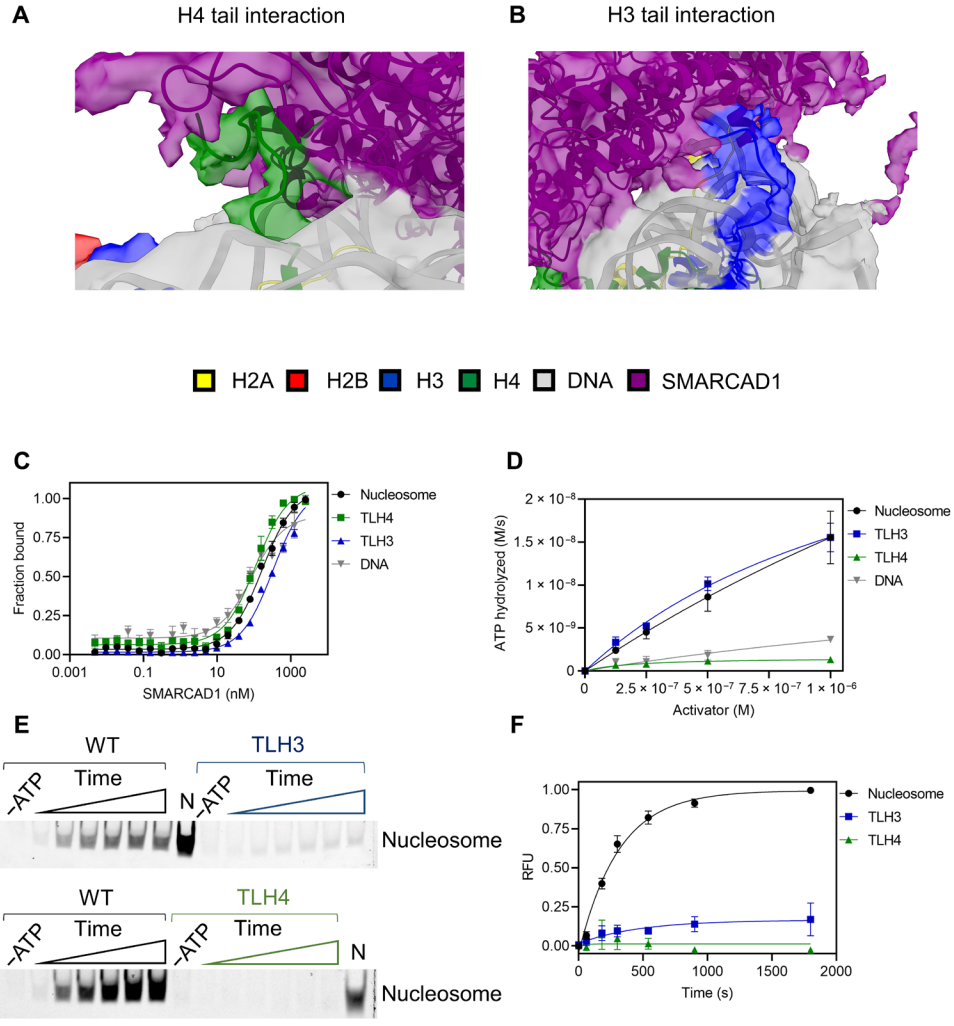

Fig. 5. Histone H3 and H4 tails are important for SMARCAD1 activity. (**A**) SMARCAD1 makes extensive contacts with the H4 tail. Cryo-EM map (transparent) with model reveals that SMARCAD1 makes several contacts with the H4 tail and (**B**) with the H3 tail. To improve clarity, the surface dust command was used in ChimeraX to remove noise from maps. (**C**) SMARCAD1 binds nucleosomes with full-length histones [wild type (WT)], as well as nucleosomes with tail-deleted histones (TLH4 and TLH3), and DNA. $K_{D,nucleosome} = 160 \pm 10$ nM, $K_{D,TLH4} = 110 \pm 10$ nM, $K_{D,TLH3} = 330 \pm 20$ nM, $K_{D,DNA} = 80 \pm 10$ nM. K_D and SE were obtained from three replicates; data for WT nucleosome and DNA are same as in Fig. 1A. (**D**) SMARCAD1 is activated by WT nucleosome and TLH3 nucleosomes equally well, but TLH4 nucleosome and DNA are poor activators of ATP hydrolysis. SE bars are from three replicates; data for WT nucleosome and DNA are same as in Fig, 1B and included for clarity here. (**E**) Histone exchange assay reveals that SMARCAD1 exchanges WT histones well, but it is unable to exchange TLH3 or TLH4 histones. Time points were 0, 60, 18, 300, 540, 900, 1800 s. (**F**) Quantification of gel from (E) confirms that SMARCAD1 poorly exchanges TLH3 or TLH4 histones compared to WT histones. SE bars in graph are from three replicates (six for WT nucleosomes).

as the template for the homology model of the SMARCAD1 ATPase domains, bind nucleosomal DNA at SHL −2 and at the neighboring gyre of the DNA superhelix (SHL 6) through ATPase 2 and ATPase 1, respectively, and is also anchored by interactions between ATPase 2 and the H4 tail (fig. S8). Intriguingly the interactions between the H4 tail and ATPase 2 appear to be maintained in SMARCAD1, but, compared to Iswi, the two domains swivel around this anchor and translate by one SHL to interact with SHL −1, SHL 0, and extranucleosomal DNA (fig. S8). SMARCAD1 interactions with the nucleosome also differ from its closest homolog INO80, which contacts DNA at SHL 6 and SHL 3, highlighting the variability in interactions of the ATPase domains with their nucleosome substrates that likely is reflected in their different functions.

The ability of SMARCAD1 to interact with the nucleosome (and with DNA) is completely inhibited by phosphorylation of its N-terminal region (Fig. 1, C and D), and only after exhaustive dephosphorylation of the 23 identified sites that are all located N-terminal to the ATPase domains is SMARCAD1 able to bind nucleosomes. It is common for remodelers to be regulated through autoinhibition (*2*), and we hypothesize that phosphorylation might regulate an autoinhibition domain. Exactly which phosphorylation sites are required for autoinhibition, and the mechanism of inhibition remains to be elucidated. Fun30 was shown to be phosphorylated in the N terminus in a cell cycle–dependent manner, and this modification is required for interaction with the scaffold protein Dpb11 (*6*). Therefore, it is possible that the phosphorylation state regulates both the activity of SMARCAD1 and its appropriate recruitment to

Downloaded from https://www.science.org on June 12, 2022

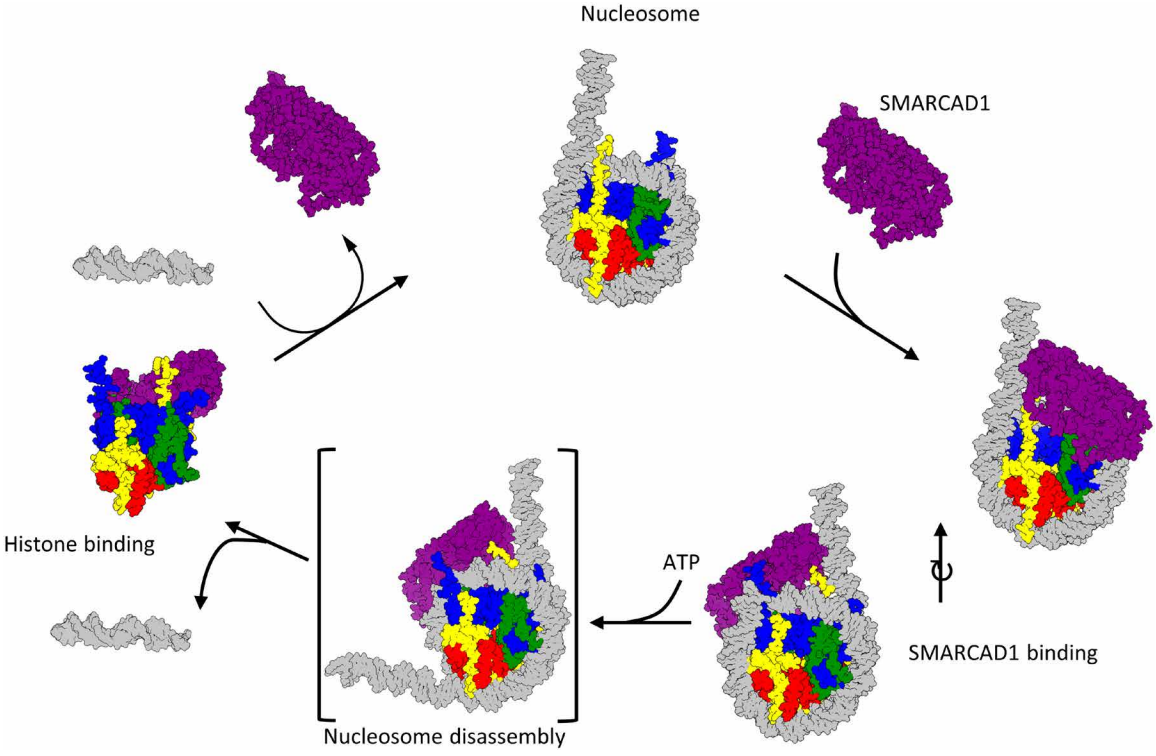

Fig. 6. Proposed model for SMARCAD1 activity SMARCAD1 first binds to the nucleosome on its proximal side by engaging extranucleosomal DNA and DNA at SHL 0 and SHL −1. SMARCAD1 then uses the energy of ATP hydrolysis to peel DNA off the distal side of the nucleosome allowing it to remove the histones. SMARCAD1 holds onto all four histones, possibly as a histone octamer, and deposits them back onto DNA to reform a nucleosome.

chromatin through phosphorylation-sensitive interactions with binding partners.

The ATP hydrolysis activity of SMARCAD1 is optimally triggered by the interaction with nucleosomes (Fig. 2B), and the energy is used to dissociate histones from DNA (Fig. 2, D and E). SMARCAD1 then deposits the histones (H3-H4 and H2A-H2B) onto a new DNA segment at the same rate. When incubated with histones in the absence of DNA, SMARCAD1 brings H4 and H2B (and, by extension, the histones H3-H4 and H2A-H2B) into close proximity (Fig. 3D). We therefore suggest that unlike Swr1 (*40*) that only exchanges histone H2A-H2B dimers, SMARCAD1 is able to transfer the entire histone octamer. A similar activity was proposed for the remodeler RSC (*5*) and suggested for Fun30 (*22*). It is entirely possible that other remodelers can also transfer the entire histone octamer, but how widespread this activity is among remodelers, under which circumstances it occurs, and what its biological functions are remain to be investigated. Further studies will address how common this histone exchange process is and how similar this particular activity is among different remodelers.

The two classes of particles obtained with the SMARCAD1-nucleosome complex described here are distinguished mainly by the amount of DNA bound on the SMARCAD1 distal side of the nucleosome (fig. S5). While in class 1, the DNA maintains all its contacts with the histone octamer, ~20 bp of DNA is peeled away from the histone octamer in class 2, and the first histone-DNA contact is at SHL +4. While this could be the result of spontaneous "breathing" (*36*), it is suggestive that the SMARCAD1 N-terminal domain, which is highly acidic and predicted to be disordered (and therefore not defined in any of the current maps), projects toward this region. We speculate that this region may protect the DNA binding surfaces of H2A-H2B that are exposed when the DNA is peeled away similar to what was observed in the FACT-nucleosome complex (*41*). Such a mechanism would prevent the rebinding of DNA and facilitate the removal of the entire histone octamer by SMARCAD1.

Together, our data suggest a mechanism (shown in Fig. 6) in which SMARCAD1 engages nucleosome by interacting with extranucleosomal DNA and the DNA near SHL 0. We propose that, in the presence of ATP, SMARCAD1 destabilizes histone-DNA interactions, thereby allowing SMARCAD1 to compete DNA away from the histone octamer. As SMARCAD1 continues to hydrolyze ATP and destabilize histone-DNA interactions, the histones become even more exposed, eventually allowing SMARCAD1 to completely remove them from DNA. Further work will focus on biochemically confirming this model with mutagenesis studies, and higher-resolution cryo-EM analysis of this and other hypothetical intermediates will further define SMARCAD1-nucleosome interactions.

Several remodelers interact with histone tails, most notably with the H4 N-terminal tail (*2*). Of particular interest, the H4 N-terminal tail relieves autoinhibition of Iswi, and this promotes ATP hydrolysis (*42*). Here, we show that SMARCAD1 interacts with both the H4 and H3 N-terminal tails (Fig. 5, A and B). The H4 tail (but not the H3 tail) is required for the ATP hydrolysis activity of SMARCAD1 (Fig. 5D), while both tails are required for histone exchange onto a new DNA fragment (Fig. 5F). We speculate that SMARCAD1 can engage nucleosomal DNA (and free DNA) but is unable to hydrolyze ATP beyond a basal level until it is properly situated on the

Downloaded from https://www.science.org on June 12, 2022

nucleosome, as read out by proper interactions with the H4 tail. Further stabilization by the H3 tail then promotes histone eviction. Histone tails are extensively posttranslationally modified, and hence, the interactions with histone tails might provide a mechanism for regulating SMARCAD1 activity.

Limitations of this study

In total, 23 phosphorylation sites were identified on Sf9-expressed SMARCAD1. While removal of phosphorylation sites allows for activation of SMARCAD1, we currently do not know which SMARCAD1 sites are important nor do we know which sites are physiologically relevant, as Sf9 is not the endogenous human SMARCAD1 expression system.

Our data suggest that SMARCAD1 removes entire histone octamer and deposits it, as a whole, onto another DNA fragment. We infer this from our finding that both H2AH2B and H3H4 are transferred at identical rates. However, it is also possible that the rate-limiting step of histone transfer comes before histone eviction, and therefore, the rate of transfer only appears to be identical for the different histones. More direct measurements of histone transfer will address this important mechanistic question. Our model is supported by our finding that SMARCAD1 brings H3H4 and H2AH2B together in the absence of DNA (by the use of FRET). However, the stoichiometry and relative orientation of the histones on SMARCAD1 have yet to be revealed and we currently do not know whether this resembles an octamer. Last, despite our best efforts, the resolution of our cryo-EM density (in particular, the SMARCAD1 portion) is too low to make definitive conclusions of SMARCAD1-nucleosome interactions. Future work will focus on obtaining higher resolution of the complex to build a well-defined model.

MATERIALS AND METHODS

Cloning and purification of SMARCAD1

A plasmid containing the human SMARCAD1 DNA sequence was purchased from DNASU. The sequence was polymerase chain reaction (PCR)–amplified to add an N-terminal 6-His tag, and restriction enzyme overhangs to allow cloning into the pACEBAC1 plasmid. Sf9 cells were infected with *Autographa californica* multiple nucleopolyhedrovirus, and virus was amplified using the Bac-to-Bac system. Generally, expression was done in 300 ml of Sf9 cells and pelleted after 3-day expression. Cells were resuspended in lysis buffer [250 mM NaCl, 20 mM Hepes (pH 7.5), 2 mM Tris(2-carboxyethyl)phosphine, 1 mM 4-(2-aminoethyl)benzenesulfonyl fluoride hydrochloride, 10% glycerol, and 2 mM $MgCl_2$] supplemented with a cOmplete Protease Inhibitor Cocktail (Roche Diagnostics) and 1500 U of Benzonase (Millipore Sigma) per 300 ml of Sf9 insect cells. Resuspended cells were lysed using a TissueLyser (Tekmar), incubated on ice for 10 min, sonicated, and spun at 31,000 RCF (Beckman JA-20 rotor) for 15 min, followed by purifications over a 5-ml nickel column, a 5-ml HiTrap-Q column, and, lastly, an S200 (GE) column.

For dephosphorylation after the HiTrap-Q column, pure fractions were mixed with 500 U of Quick Calf Intestinal Alkaline Phosphatase (New England BioLabs) per 1-mg SMARCAD1 for 1 hour at room temperature. The sample was purified over a 1-ml nickel column followed by gel filtration over an S200 column. Both phosphorylated and dephosphorylated samples were frozen in S200 buffer [100 mM KCl, 20 mM Hepes (pH 7.5), 2 mM TCEP, 1 mM AEBSF, and 10% glycerol]. Yield was in the range of 5 to 10 mg from 300 ml of Sf9 cells.

Size exclusion chromatography coupled to multiangle light scattering

SEC-MALS was performed nearly the same as previously described with a few changes (*43*). pSMARCAD1 was concentrated to 15.9 μM and injected onto a Superdex 200 (S200) Increase 10/300 size exclusion column equilibrated in 100 mM KCl, 20 mM Hepes (pH 7.5), and 2 mM TCEP. Light scattering and refractive index of the eluate were measured with a Dawn Heleos-II instrument (Wyatt Technology) and an Optilab rEX instrument (Wyatt Technology). Data were processed in Astra version 6 software (Wyatt Technology).

Mass spectrometry and analysis of SMARCAD1 phosphorylation sites

One-microgram SMARCAD1 was digested with 1 U of trypsin (Thermo Fisher Scientific), cleaned up with Pierce C-18 columns (Thermo Fisher Scientific), and sent to the mass spectrometry facility at University of Colorado Boulder. Raw files were searched in the Max-Quant software (MaxQuant) using a SMARCAD1 Fasta file. We enriched for phosphorylation sites by using the phosphorylation (STY) modification. Identified phosphorylation sites are indicated in Fig. 1B.

Histone refolding and nucleosome reconstitution

Human histones were purchased from the Histone Source at Colorado State University (Fort Collins) and refolded, and DNA was obtained as previously described (*44*). E63C H4 was labeled with a maleimide–Alexa Fluor 488 fluorophore, and T115C H2B was either labeled with a maleimide–Alexa Fluor 488 or a maleimide-Atto647N fluorophore, as indicated (*45*). For TL histone experiments, TLH3 (38 to 135) or TLH4 (20 to 102) were reconstituted the same as WT histones.

DNA for nucleosomes to be used for cryo-EM was made from 10-ml PCRs using in-house purified Pfu-polymerase. The following DNA sequence was used (601 nucleosome positioning sequence in bold):

ATCTGAGAATCCGGTGCCGAGGCCGCTCAATTGGTC-GTAGACAGCTCTAGCACCGCTTAAACGCACGTACGC-GCTGTCCCCCGCGTTTTAACCGCCAAGGGGATTACTC-CCTAGTCTCCAGGCACGTGTCAGATATATACATCCGAT-ATCGGATCCTCTAGAGTCGACCTGCAGGCATG-CAAGCTTGGCGTAATCATGGTCATAGCTGTTTCCTGTG.

Nucleosomes were reconstituted as described (*44*).

Nucleosome FP

SMARCAD1 binding to nucleosomes was determined using an FP assay. Assays were done in binding buffer [20 mM tris-Cl (pH 7.5), 2 mM dithiothreitol (DTT), 1 mM EDTA, 0.01% CHAPS, and 0.01% NP-40]. Alexa Fluor 488–labeled H4 nucleosomes were used at a final concentration of 10 nM. SMARCAD1 was mixed with nucleosomes at increasing concentrations from 0 to 2500 nM in nucleosome binding buffer. The increase in FP values as a function of SMARCAD1 concentration was measured in a BMG Labtech CLARIOstar plate reader. For the DNA binding experiments, DNA was made by PCR amplifying 147-bp 601 sequence with primers containing Alexa Fluor 488 label [purchased from Integrated DNA Technologies (IDT)]. All FP binding curves were fit to the quadratic binding equation

Downloaded from https://www.science.org on June 12, 2022

$$Y = Y_{min} + (Y_{max} - Y_{min}) \times (K_d + L + X\text{-sqrt}(\text{sqr}(K_d + L + X) - (4 \times L \times X))) / 2 \times L$$

where Y_{min} and Y_{max} are the minimum and maximum FP Y signals, respectively, K_d is the experimental binding constant, L is the ligand concentration (10 nM), and X is the SMARCAD1 concentration.

ATP hydrolysis assay

We used an assay that couples ATP hydrolysis to NADH oxidation using lactate dehydrogenase (LDH) and pyruvate kinase (PK) (*4*). The reaction was done in ATP hydrolysis buffer (1 mM DTT, 4 mM $MgCl_2$, 1 mM phosphoenolpyruvate, and 12 μl of LDH/PK enzyme mix (Sigma-Aldrich), 50 mM Hepes (pH 7.5), 100 mM KCl, and 0.7 mM NADH). One hundred–microliter reactions were conducted by mixing 100 nM SMARCAD1, ATP hydrolysis buffer, and increasing amounts of activator and then initiated by addition of 1 mM ATP. Reactions were measured in a BMG Labtech CLARIOstar plate reader, where NADH absorbance was measured at a wavelength of 340 nm. Rates were obtained from slopes of simple linear regression. Change in A340/s was converted to ATP hydrolyzed ([M]/s) by using the NADH extinction coefficient (6330 M^{-1} cm^{-1}). Background ATP hydrolysis (SMARCAD1 without activator) was subtracted, and then rates as a function of activator concentration were plotted and fit to the Michaelis-Menten equation

$$Y = V_{max} \times X(K_m + X)$$

Histone exchange assay

Trinucleosomes (30N60N60N30; the numbers refer to base pair linker DNA, while N refers to 147-bp 601 nucleosome; Fig. 2C) were created in the same way as above with H2B or H4 labeled with Atto647N. Histone exchange assays were done at 3 μM SMARCAD1, 62.5 nM trinucleosomes (equivalent to 225 nM individual nucleosomes), and 1.5 μM acceptor 0 N0 DNA and conducted in 2 mM DTT, 2 mM $MgCl_2$, 25 mM Hepes (pH 7.5), and 50 mM KCl. Reactions were started with addition of 1 mM ATP and, at the appropriate time points, were quenched with quench buffer (final concentration 68 mM EDTA and 16% glycerol). Samples were analyzed on 5% native tris-borate EDTA (TBE) gels, imaged on Typhoon imager, and then quantified with ImageQuant. Rates were calculated using a one-phase association equation

$$Y = Y0 + (\text{Plateau} - Y0) \times (1\text{-exp}(-K^*))$$

FP-based quantification of SMARCAD1-histone interactions

We used the FP assay to determine whether SMARCAD1 binds H3-H4 and H2A-H2B individually in the absence of DNA. Alexa Fluor 488–H3-H4 (5 nM) or Alexa Fluor 488–H2A-H2B (5 nM) in 2 mM DTT, 10% glycerol, 50 mM Hepes (pH 7.5), 0.01% CHAPS, 0.01% NP-40, and 300 mM KCl was combined with increasing concentrations of SMARCAD1 (0 to 2.5 μM). The increase in FP signal as a function of SMARCAD1 concentration was determined in a BMG Labtech CLARIOstar plate reader, where no SMARCAD1 H3-H4 signal was arbitrarily set at an FP value of 100 mP. Binding constants were calculated using a hyperbolic binding equation

$$Y = Y_{min} + (Y_{max} - Y_{min}) \times [\text{SMARCAD1}] / (K_D + [\text{SMARCAD1}])$$

FRET-based SMARCAD1-histone interactions

To determine whether SMARCAD1 binds to histones H2A-H2B and H3-H4 simultaneously in the absence of DNA, we used a FRET-based approach that allows us to monitor (H3-H4) interactions with (H2A-H2B). Refolded Alexa Fluor 488–H3-H4 and Atto647N-H2A-H2B histones were mixed at low concentration (10 nM) in 2 mM DTT, 2 mM $MgCl_2$, 50 mM Hepes (pH 7.5), 0.01% CHAPS, and 0.01% NP-40. SMARCAD1 was added at increasing concentration (0 to 125 nM). The increase in FRET values as a function of SMARCAD1 concentration was measured in a BMG Labtech CLARIOstar plate reader, where highest SMARCAD1 titration points were arbitrarily set at 50% fluorescent intensity. Binding constants were calculated using a hyperbolic binding equation

$$Y = Y_{min} + (Y_{max} - Y_{min}) \times [\text{SMARCAD1}] / (K_D + [\text{SMARCAD1}])$$

SMARCAD1 de novo nucleosome assembly assay

To monitor whether SMARCAD1 assembles nucleosomes de novo, we used an assay that monitors incorporation of histones onto DNA as more SMARCAD1 is added. SMARCAD1 (indicated concentrations) was mixed with H3-H4 (50 nM) and H2A-H2B (Atto647N H2B; 50 nM) for 15 min in 2 mM DTT, 100 mM KCl, 50 mM Hepes (pH 7.5), 10% glycerol, and 2 mM $MgCl_2$. A total of 147-bp DNA (50 nM) was added (with 1 mM ATP when indicated) for 15 min. Samples were quenched with 16% glycerol, 68 mM EDTA, and 2.7 μg of pUC19 plasmid. Reactions were analyzed by a 5% native TBE gel, imaged on a Typhoon imager, and then quantified with ImageQuant.

Cryo-EM SMARCAD1-nucleosome sample preparation

To prepare SMARCAD1-nucleosome complex for cryo-EM, we first reconstituted a 0 N70 nucleosome using published procedures (*44*). We then combined SMARCAD1 (final concentration 16 μM) with 0 N70 nucleosome (2 μM) in S200 buffer. For cross-linking, GraFix buffers with top buffer [10% glycerol, 50 mM NaCl, 10 mM Hepes (pH 7), 1 mM $MgCl_2$, 500 μM ADP, 8 mM NaF, and 1 mM $BeSO_4$] and bottom buffer [30% glycerol, 50 mM NaCl, 10 mM Hepes (pH 7), 1 mM $MgCl_2$, 500 μM ADP, 8 mM NaF, 1 mM $BeSO_4$, and 0.15% glutaraldehyde] were used. A 10 to 30% glycerol gradient was generated, and 200 μl of SMARCAD1-nucleosome sample was added to the top. Samples were spun at 28 K rpm in an sw40-TI rotor (Beckman) for 20 hours in an ultracentrifuge. Fractions were collected and analyzed by TBE and SDS-PAGE, and fractions containing complex were collected. They were then dialyzed into 50 mM NaCl, 10 mM tris (pH 8), 2 mM $MgCl_2$, 1 mM ADP, 16 mM NaF, 2 mM $BeSO_4$, and 3 mM DTT (*32*, *33*).

Cryo-EM grid preparation and data collection

Four microliters of dialyzed sample was deposited onto glow-discharged C-flat Au 1.2/1.3 grids (Electron Microscopy Sciences) and flash-frozen using a manual plunger. Grids were screened at the University of Colorado Boulder Cryo-EM facility using a Tecnai T20 microscope with a K3 electron detector. High-quality grids were then sent to the Janelia Research Campus cryo-EM facility for data acquisition. The complex was imaged at a magnification of ×64000 on an FEI Titan Krios (300 kV) equipped with a Gatan K3 summit direct detector. Pixel size was 1.065 Å. The movies were captured in super-resolution mode with an electron dose rate at 7.8 electrons per pixel

Downloaded from https://www.science.org on June 12, 2022

per second for 5.593 s at 0.13 s per frame. The defocus range was −1.2 to −2.5 μm. A total of 11,160 images were collected.

Cryo-EM processing and model building

The data were processed in two separate steps. In the first round of processing, most images were removed because of poor Contrast Transfer Function (CTF) fits. The remaining 2408 movies were patch motion–corrected and patch CTF–corrected in cryoSPARC version 2.4 (*46*). Particles were then picked with the cryoSPARC blob picker and extracted at a box size of 256 A^2. Extracted particles were subjected to two-dimensional (2D) classification, and then good classes were used as templates in the cryoSPARC template picker. The template picker resulted in 1,513,927 particles. These were subjected to 2D classification in cryoSPARC, and bad particles were removed resulting in 440,777 particles. These particles were then transferred to RELION version 3.0 for further processing (*47*). Using an initial model from 10,184 particles, all particles were subjected to two rounds of 3D classification. After 3D classification, we had 320,523 particles present in one class. These particles could not be cleaned up further even when the initial model was low pass–filtered to 30 Å. To increase the resolution of the SMARCAD1 density, a mask was created that only encompassed the SMARCAD1 region. With this mask, particles were further subjected to two rounds of 3D classification without image alignment. Best particles were then subjected to 3D refinement, which resulted in a final resolution of 6.49 Å [Fourier Shell Correlation (FSC) = 0.143]. FSC curves were determined with the 3D FSC server (*48*).

In the second round of processing, 5395 movies were patch motion–corrected and patch CTF–corrected in cryoSPARC. Using the same templates from the first round of processing, a total of 3,282,892 particles were picked. These were subjected to one round of 2D classification in cryoSPARC, which resulted in 943,877 particles. These were brought to RELION, where they underwent two rounds of 3D classification. A third round of 3D classification was performed with local angular searches, which revealed a new SMARCAD1-nucleosome class, showing DNA peeled away from the histone core. This class was further processed and autorefined to a resolution of 6.2 Å (FSC = 0.143).

For the nucleosome, model building was performed by placing the human nucleosome (PDB: 2CV5) into the density. We manually built the DNA into the density using Coot (*49*). As noted in the results, the density for SMARCAD1 is at lower resolution than the nucleosome because of its high flexibility. Therefore, it was difficult to manually build the SMARCAD1 structure. To aid in SMARCAD1 model building, we first used SWISS-MODEL to predict a structure of SMARCAD1. Iswi (PDB: 5JXR) was used as a template because it had the highest QMEAN score (−2.46) and overall best sequence coverage (42.08%) (*35*). The predicted structure was then docked into the EM map in chimera (*50*). To better fit the model into the density map, the structure and map were run in Flex-EM (*51*). The model was then simulated in Molecular Dynamics Flexible Fitting (MDFF) [using the Nanoscale Molecular Dynamics (NAMD) engine and visualized in Visual Molecular Dynamics (VMD)], and then further processed in Interactive Structure Optimization by Local Direct (ISOLDE) to further increase model to map fitting (*52*–*55*).

Statistical analysis

All experiments were performed at least in triplicate (as indicated in each figure). All data (besides mass spectrometry) were analyzed and plotted in GraphPad Prism.

SUPPLEMENTARY MATERIALS

Supplementary material for this article is available at https://science.org/doi/10.1126/sciadv.abk2380

View/request a protocol for this paper from *Bio-protocol*.

REFERENCES AND NOTES

1. K. Luger, A. W. Mäder, R. K. Richmond, D. F. Sargent, T. J. Richmond, Crystal structure of the nucleosome core particle at 2.8 Å resolution. *Nature* **389**, 251–260 (1997).
2. J. Markert, K. Luger, Nucleosomes meet their remodeler match. *Trends Biochem. Sci.* **46**, 41–50 (2021).
3. R. K. Singh, J. Fan, N. Gioacchini, S. Watanabe, O. Bilsel, C. L. Peterson, Transient kinetic analysis of SWR1C-Catalyzed H2A.Z deposition unravels the impact of nucleosome dynamics and the asymmetry of histone exchange. *Cell Rep.* **27**, 374–386.e4 (2019).
4. S. Eustermann, K. Schall, D. Kostrewa, K. Lakomek, M. Strauss, M. Moldt, K. P. Hopfner, Structural basis for ATP-dependent chromatin remodelling by the INO80 complex. *Nature* **556**, 386–390 (2018).
5. C. E. Rowe, G. J. Narlikar, The ATP-dependent remodeler RSC transfers histone dimers and octamers through the rapid formation of an unstable encounter intermediate. *Biochemistry* **49**, 9882–9890 (2010).
6. S. C. Bantele, P. Ferreira, D. Gritenaite, D. Boos, B. Pfander, Targeting of the Fun30 nucleosome remodeller by the Dpb11 scaffold facilitates cell cycle-regulated DNA end resection. *eLife* **6**, (2017).
7. S. Chakraborty, R. K. Pandita, S. Hambarde, A. R. Mattoo, V. Charaka, K. M. Ahmed, S. P. Iyer, C. R. Hunt, T. K. Pandita, SMARCAD1 phosphorylation and ubiquitination are required for resection during DNA double-strand break repair. *iScience* **2**, 123–135 (2018).
8. T. Costelloe, R. Louge, N. Tomimatsu, B. Mukherjee, E. Martini, B. Khadaroo, K. Dubois, W. W. Wiegant, A. Thierry, S. Burma, H. van Attikum, B. Llorente, The yeast Fun30 and human SMARCAD1 chromatin remodellers promote DNA end resection. *Nature* **489**, 581–584 (2012).
9. R. M. Densham, A. J. Garvin, H. R. Stone, J. Strachan, R. A. Baldock, M. Daza-Martin, A. Fletcher, S. Blair-Reid, J. Beesley, B. Johal, L. H. Pearl, R. Neely, N. H. Keep, F. Z. Watts, J. R. Morris, Human BRCA1-BARD1 ubiquitin ligase activity counteracts chromatin barriers to DNA resection. *Nat. Struct. Mol. Biol.* **23**, 647–655 (2016).
10. M. Doiguchi, T. Nakagawa, Y. Imamura, M. Yoneda, M. Higashi, K. Kubota, S. Yamashita, H. Asahara, M. Iida, S. Fujii, T. Ikura, Z. Liu, T. Nandu, W. L. Kraus, H. Ueda, T. Ito, SMARCAD1 is an ATP-dependent stimulator of nucleosomal H2A acetylation via CBP, resulting in transcriptional regulation. *Sci. Rep.* **6**, 20179 (2016).
11. N. Okazaki, S. Ikeda, R. Ohara, K. Shimada, T. Yanagawa, T. Nagase, O. Ohara, H. Koga, The novel protein complex with SMARCAD1/KIAA1122 binds to the vicinity of TSS. *J. Mol. Biol.* **382**, 257–265 (2008).
12. S. P. Rowbotham, L. Barki, A. Neves-Costa, F. Santos, W. Dean, N. Hawkes, P. Choudhary, W. R. Will, J. Webster, D. Oxley, C. M. Green, P. Varga-Weisz, J. E. Mermoud, Maintenance of silent chromatin through replication requires SWI/SNF-like chromatin remodeler SMARCAD1. *Mol. Cell* **42**, 285–296 (2011).
13. Y. Takeishi, R. Fujikane, M. Rikitake, Y. Obayashi, M. Sekiguchi, M. Hidaka, SMARCAD1-mediated recruitment of the DNA mismatch repair protein MutLα to MutSα on damaged chromatin induces apoptosis in human cells. *J. Biol. Chem.* **295**, 1056–1065 (2020).
14. R. Terui, K. Nagao, Y. Kawasoe, K. Taki, T. L. Higashi, S. Tanaka, T. Nakagawa, C. Obuse, H. Masukata, T. S. Takahashi, Nucleosomes around a mismatched base pair are excluded via an Msh2-dependent reaction with the aid of SNF2 family ATPase Smarcad1. *Genes Dev.* **32**, 806–821 (2018).
15. K. Arafat, E. al Kubaisy, S. Sulaiman, S. M. Karam, Z. al Natour, A. H. Hassan, S. Attoub, SMARCAD1 in breast cancer progression. *Cell. Physiol. Biochem.* **50**, 489–500 (2018).
16. F. Liu, Z. Xia, M. Zhang, J. Ding, Y. Feng, J. Wu, Y. Dong, W. Gao, Z. Han, Y. Liu, Y. Yao, D. Li, SMARCAD1 promotes pancreatic cancer cell growth and metastasis through Wnt/β-catenin-Mediated EMT. *Int. J. Biol. Sci.* **15**, 636–646 (2019).
17. A. Flaus, D. M. Martin, G. J. Barton, T. Owen-Hughes, Identification of multiple distinct Snf2 subfamilies with conserved structural motifs. *Nucleic Acids Res.* **34**, 2887–2905 (2006).
18. G. J. Narlikar, R. Sundaramoorthy, T. Owen-Hughes, Mechanisms and functions of ATP-dependent chromatin-remodeling enzymes. *Cell* **154**, 490–503 (2013).
19. D. Ding, P. Bergmaier, P. Sachs, M. Klangwart, T. Rückert, N. Bartels, J. Demmers, M. Dekker, R. A. Poot, J. E. Mermoud, The CUE1 domain of the SNF2-like chromatin remodeler SMARCAD1 mediates its association with KRAB-associated protein 1 (KAP1) and KAP1 target genes. *J. Biol. Chem.* **293**, 2711–2724 (2018).
20. M. Lim, J. A. Newman, H. L. Williams, L. Masino, H. Aitkenhead, A. E. Gravard, O. Gileadi, J. Q. Svejstrup, A ubiquitin-binding domain that binds a structural fold distinct from that of ubiquitin. *Structure* **27**, 1316–1325.e6 (2019).

Downloaded from https://www.science.org on June 12, 2022

21. P. Sachs, D. Ding, P. Bergmaier, B. Lamp, C. Schlagheck, F. Finkernagel, A. Nist, T. Stiewe, J. E. Mermoud, SMARCAD1 ATPase activity is required to silence endogenous retroviruses in embryonic stem cells. *Nat. Commun.* **10**, 1335 (2019).
22. C. Navarro, J. Lyu, A. M. Katsori, R. Caridha, S. J. Elsasser, An embryonic stem cell-specific heterochromatin state promotes core histone exchange in the absence of DNA accessibility. *Nat. Commun.* **11**, 5095 (2020).
23. J. Lee, E. Shik Choi, H. David Seo, K. Kang, J. M. Gilmore, L. Florens, M. P. Washburn, J. Choe, J. L. Workman, D. Lee, Chromatin remodeller Fun30Fft3 induces nucleosome disassembly to facilitate RNA polymerase II elongation. *Nat. Commun.* **8**, 14527 (2017).
24. X. Chen, D. Cui, A. Papusha, X. Zhang, C. D. Chu, J. Tang, K. Chen, X. Pan, G. Ira, The Fun30 nucleosome remodeller promotes resection of DNA double-strand break ends. *Nature* **489**, 576–580 (2012).
25. A. Neves-Costa, W. R. Will, A. T. Vetter, J. R. Miller, P. Varga-Weisz, The SNF2-family member Fun30 promotes gene silencing in heterochromatic loci. *PLOS ONE* **4**, e8111 (2009).
26. B. Steglich, A. Strålfors, O. Khorosjutina, J. Persson, A. Smialowska, J. P. Javerzat, K. Ekwall, The Fun30 chromatin remodeler Fft3 controls nuclear organization and chromatin structure of insulators and subtelomeres in fission yeast. *PLOS Genet.* **11**, e1005101 (2015).
27. N. Taneja, M. Zofall, V. Balachandran, G. Thillainadesan, T. Sugiyama, D. Wheeler, M. Zhou, S. I. S. Grewal, SNF2 family protein Fft3 suppresses nucleosome turnover to promote epigenetic inheritance and proper replication. *Mol. Cell* **66**, 50–62.e6 (2017).
28. C. S. Y. Lo, M. van Toorn, V. Gaggioli, M. Paes Dias, Y. Zhu, E. M. Manolika, W. Zhao, M. van der Does, C. Mukherjee, J. G. S. C. Souto Gonçalves, M. E. van Royen, P. J. French, J. Demmers, I. Smal, H. Lans, D. Wheeler, J. Jonkers, A. R. Chaudhuri, J. A. Marteijn, N. Taneja, SMARCAD1-mediated active replication fork stability maintains genome integrity. *Sci. Adv.* **7**, eabe7804 (2021).
29. S. Awad, D. Ryan, P. Prochasson, T. Owen-Hughes, A. H. Hassan, The Snf2 homolog Fun30 acts as a homodimeric ATP-dependent chromatin-remodeling enzyme. *J. Biol. Chem.* **285**, 9477–9484 (2010).
30. S. Sif, P. T. Stukenberg, M. W. Kirschner, R. E. Kingston, Mitotic inactivation of a human SWI/SNF chromatin remodeling complex. *Genes Dev.* **12**, 2842–2851 (1998).
31. L. C. Lehmann, G. Hewitt, S. Aibara, A. Leitner, E. Marklund, S. L. Maslen, V. Maturi, Y. Chen, D. van der Spoel, J. M. Skehel, A. Moustakas, S. J. Boulton, S. Deindl, Mechanistic insights into autoinhibition of the oncogenic chromatin remodeler ALC1. *Mol. Cell* **68**, 847–859.e7 (2017).
32. H. Stark, GraFix: Stabilization of fragile macromolecular complexes for single particle cryo-EM. *Methods Enzymol.* **481**, 109–126 (2010).
33. X. Liu, M. Li, X. Xia, X. Li, Z. Chen, Mechanism of chromatin remodelling revealed by the Snf2-nucleosome structure. *Nature* **544**, 440–445 (2017).
34. R. Ren, S. Ghassabi Kondalaji, G. D. Bowman, The Chd1 chromatin remodeler forms long-lived complexes with nucleosomes in the presence of ADP.BeF_3^- and transition state analogs. *J. Biol. Chem.* **294**, 18181–18191 (2019).
35. T. Schwede, J. Kopp, N. Guex, M. C. Peitsch, SWISS-MODEL: An automated protein homology-modeling server. *Nucleic Acids Res.* **31**, 3381–3385 (2003).
36. S. Bilokapic, M. Strauss, M. Halic, Histone octamer rearranges to adapt to DNA unwrapping. *Nat. Struct. Mol. Biol.* **25**, 101–108 (2018).
37. L. R. Racki, N. Naber, E. Pate, J. D. Leonard, R. Cooke, G. J. Narlikar, The histone H4 tail regulates the conformation of the ATP-binding pocket in the SNF2h chromatin remodeling enzyme. *J. Mol. Biol.* **426**, 2034–2044 (2014).
38. J. Ludwigsen, S. Pfennig, A. K. Singh, C. Schindler, N. Harrer, I. Forné, M. Zacharias, F. Mueller-Planitz, Concerted regulation of ISWI by an autoinhibitory domain and the H4 N-terminal tail. *eLife* **6**, (2017).
39. W. L. Hwang, S. Deindl, B. T. Harada, X. Zhuang, Histone H4 tail mediates allosteric regulation of nucleosome remodelling by linker DNA. *Nature* **512**, 213–217 (2014).
40. O. Willhoft, M. Ghoneim, C. L. Lin, E. Y. D. Chua, M. Wilkinson, Y. Chaban, R. Ayala, E. A. McCormack, L. Ocloo, D. S. Rueda, D. B. Wigley, Structure and dynamics of the yeast SWR1-nucleosome complex. *Science* **362**, eaat7716 (2018).
41. Y. Liu, K. Zhou, N. Zhang, H. Wei, Y. Z. Tan, Z. Zhang, B. Carragher, C. S. Potter, S. D'Arcy, K. Luger, FACT caught in the act of manipulating the nucleosome. *Nature* **577**, 426–431 (2020).
42. C. R. Clapier, B. R. Cairns, Regulation of ISWI involves inhibitory modules antagonized by nucleosomal epitopes. *Nature* **492**, 280–284 (2012).
43. G. Gaullier, G. Roberts, U. M. Muthurajan, S. Bowerman, J. Rudolph, J. Mahadevan, A. Jha, P. S. Rae, K. Luger, Bridging of nucleosome-proximal DNA double-strand breaks by PARP2 enhances its interaction with HPF1. *PLOS ONE* **15**, e0240932 (2020).
44. P. N. Dyer, R. S. Edayathumangalam, C. L. White, Y. Bao, S. Chakravarthy, U. M. Muthurajan, K. Luger, Reconstitution of nucleosome core particles from recombinant histones and DNA. *Methods Enzymol.* **375**, 23–44 (2004).
45. U. M. Muthurajan, F. Mattiroli, S. Bergeron, K. Zhou, Y. Gu, S. Chakravarthy, P. Dyer, T. Irving, K. Luger, In vitro chromatin assembly: Strategies and quality control. *Methods Enzymol.* **573**, 3–41 (2016).
46. A. Punjani, J. L. Rubinstein, D. J. Fleet, M. A. Brubaker, cryoSPARC: Algorithms for rapid unsupervised cryo-EM structure determination. *Nat. Methods* **14**, 290–296 (2017).
47. J. Zivanov, T. Nakane, B. O. Forsberg, D. Kimanius, W. J. H. Hagen, E. Lindahl, S. H. W. Scheres, New tools for automated high-resolution cryo-EM structure determination in RELION-3. *eLife* **7**, e42166 (2018).
48. Y. Z. Tan, P. R. Baldwin, J. H. Davis, J. R. Williamson, C. S. Potter, B. Carragher, D. Lyumkis, Addressing preferred specimen orientation in single-particle cryo-EM through tilting. *Nat. Methods* **14**, 793–796 (2017).
49. P. Emsley, B. Lohkamp, W. G. Scott, K. Cowtan, Features and development of Coot. *Acta Crystallogr. D Biol. Crystallogr.* **66**, 486–501 (2010).
50. E. F. Pettersen, T. D. Goddard, C. C. Huang, G. S. Couch, D. M. Greenblatt, E. C. Meng, T. E. Ferrin, UCSF Chimera—A visualization system for exploratory research and analysis. *J. Comput. Chem.* **25**, 1605–1612 (2004).
51. A. P. Joseph, S. Malhotra, T. Burnley, C. Wood, D. K. Clare, M. Winn, M. Topf, Refinement of atomic models in high resolution EM reconstructions using Flex-EM and local assessment. *Methods* **100**, 42–49 (2016).
52. T. I. Croll, ISOLDE: A physically realistic environment for model building into low-resolution electron-density maps. *Acta Crystallogr. D Struct. Biol.* **74**, 519–530 (2018).
53. W. Humphrey, A. Dalke, K. Schulten, VMD: Visual molecular dynamics. *J. Mol. Graph.* **14**, 33–38 (1996).
54. J. C. Phillips, D. J. Hardy, J. D. C. Maia, J. E. Stone, J. V. Ribeiro, R. C. Bernardi, R. Buch, G. Fiorin, J. Hénin, W. Jiang, R. McGreevy, M. C. R. Melo, B. K. Radak, R. D. Skeel, A. Singharoy, Y. Wang, B. Roux, A. Aksimentiev, Z. Luthey-Schulten, L. V. Kalé, K. Schulten, C. Chipot, E. Tajkhorshid, Scalable molecular dynamics on CPU and GPU architectures with NAMD. *J. Chem. Phys.* **153**, 044130 (2020).
55. L. G. Trabuco, E. Villa, K. Mitra, J. Frank, K. Schulten, Flexible fitting of atomic structures into electron microscopy maps using molecular dynamics. *Structure* **16**, 673–683 (2008).

Acknowledgments: We thank the Janelia Research Campus Cryo-Electron Microscopy team, especially Z. Yu, S. Yang, and X. Zhao for data collection. We also thank G. Morgan at the University of Colorado Boulder Electron Microscopy core for help with grid screening. **Funding:** This work was funded by the Howard Hughes Medical Institute. **Author contributions:** K.L. and J.M. conceived experimental design. J.M. performed all biochemical experiments and analysis. J.M. prepared cryo-EM samples. K.Z. prepared cryo-EM grids. K.Z. and J.M. conducted initial grid cryo-EM screening. J.M. analyzed cryo-EM data and performed model building. K.L. and J.M. wrote manuscript with contributions from K.Z. **Competing interests:** The authors declare that they have no competing interests. **Data and materials availability:** Maps have been deposited at EMDB (EMDB# D_1000258795 and D_1000258799), and the pdb file of the model is attached as supplementary material. All other data needed to evaluate the conclusions in the paper are present in the paper and/or the Supplementary Materials.

Submitted 30 June 2021
Accepted 20 August 2021
Published 15 October 2021
10.1126/sciadv.abk2380

Citation: J. Markert, K. Zhou, K. Luger, SMARCAD1 is an ATP-dependent histone octamer exchange factor with de novo nucleosome assembly activity. *Sci. Adv.* **7**, eabk2380 (2021).

Downloaded from https://www.science.org on June 12, 2022

ScienceAdvances

SMARCAD1 is an ATP-dependent histone octamer exchange factor with de novo nucleosome assembly activity

Jonathan MarkertKeda ZhouKarolin Luger

Sci. Adv., 7 (42), eabk2380. • DOI: 10.1126/sciadv.abk2380

View the article online
https://www.science.org/doi/10.1126/sciadv.abk2380
Permissions
https://www.science.org/help/reprints-and-permissions

Downloaded from https://www.science.org on June 12, 2022

Use of this article is subject to the Terms of service

Science Advances (ISSN) is published by the American Association for the Advancement of Science. 1200 New York Avenue NW, Washington, DC 20005. The title *Science Advances* is a registered trademark of AAAS.
Copyright © 2021 The Authors, some rights reserved; exclusive licensee American Association for the Advancement of Science. No claim to original U.S. Government Works. Distributed under a Creative Commons Attribution NonCommercial License 4.0 (CC BY-NC).